Erythro-myeloid progenitors contribute endothelial cells to blood vessels

Erythro-myeloid progenitors contribute endothelial cells to blood vessels

Alice Plein[1,*], Alessandro Fantin[1,*], Laura Denti[1], Jeffrey W. Pollard[2] and Christiana Ruhrberg[1^]

[1] UCL Institute of Ophthalmology, University College London, 11-43 Bath Street, London EC1V 9EL, UK

[2] MRC Centre for Reproductive Health, University of Edinburgh, 47 Little France Crescent, Edinburgh EH16 4TJ, UK

*contributed equally

^Corresponding author:

Professor Christiana Ruhrberg, Tel.: 44 (0)20 7608 4017; email: c.ruhrberg@ucl.ac.uk

The earliest blood vessels in the mammalian embryo are formed when endothelial cells (ECs) differentiate from angioblasts and coalesce into tubular networks. Thereafter, the endothelium is thought to expand solely by proliferation of pre-existing ECs. Here we show that the earliest precursors of erythrocytes, megakaryocytes and macrophages, the yolk sac-derived erythro-myeloid progenitors (EMPs), provide a complementary source of ECs that are recruited into pre-existing vasculature. Whereas a first wave of yolk sac-resident EMPs contributes ECs to the yolk sac endothelium, a second wave of EMPs colonises the embryo and contributes ECs to intraembryonic endothelium in multiple organs, where they persist into adulthood. By demonstrating that EMPs constitute a hitherto unrecognised and non-redundant source of ECs, we reveal that embryonic blood vascular endothelium expands in a dual mechanism that involves both the proliferation of pre-existing ECs and the incorporation of ECs derived from hematopoietic precursors.

Blood vessels distribute oxygen, nutrients, hormones and immune cells through the vertebrate body and help remove waste molecules. Accordingly, functional blood vessel formation during embryogenesis is a prerequisite for vertebrate life. Endothelial cells (ECs) form the inner lining of blood vessels to contain the blood and its constituents. In addition, ECs serve as signalling hubs to integrate tissue-derived and blood-borne signals to regulate vascular function. In the mammalian embryo, the first ECs arise from mesenchymal precursors termed angioblasts that condense into yolk sac vasculature and the paired dorsal aortae; this process is initiated on embryonic day (E) 7.0 in mice [1]. Subsequently, embryonic blood vascular endothelium is thought to expand in a process termed angiogenesis, in which ECs proliferate within existing endothelium to increase vascular diameter, extend sprouts into avascular tissue areas or remodel into smaller vessels by intussusceptive growth [1]. Current consensus is therefore that embryonic ECs are a self-contained

cell lineage that expands by proliferation without contribution from new angioblasts or circulating precursors. In contrast, circulating endothelial progenitors and their relationship to monocytes and macrophages have controversially been described in adults [2].

Monocytes and macrophages are mononuclear phagocytic cells of the innate immune system that also modulate vascular growth [3]. Thus, tissue-resident macrophages of the embryonic mouse central nervous system (CNS), termed microglia, and macrophages in the zebrafish larval trunk contact ECs at the tip of neighbouring vessel sprouts to promote their anastomosis into perfused vessel loops [4, 5]. Microglia have similar roles in the injured adult zebrafish brain [6]. Macrophages also secrete VEGFA to stimulate vessel growth for nerve repair in adult mice [7]. In contrast, a direct contribution of macrophages or other myeloid cell (MC) types to embryonic vascular endothelium has not been reported; thus, CRE recombinase expression under the control of the myeloid *Lysm* or *Vav* promoters does not mark embryonic blood vascular endothelium in mice [8, 9].

Most tissue-resident macrophages arise from erythro-myeloid progenitors (EMPs) that form in the extra-embryonic yolk sac during embryogenesis and also serve as precursors for erythrocytes and megakaryocytes [10-14]. In mice, a wave of early EMPs, also referred to as primitive progenitors, buds from yolk sac blood islands between E7.0 and E8.25 and by E9.0 differentiates into yolk sac macrophages without monocytic intermediates [10, 13, 15-17]. Early yolk sac macrophages also generate tissue-resident macrophages in the embryo proper, including microglia in the brain or Langerhans cells and Kupffer cells in the epidermis and liver, respectively [16]. A later wave of EMPs buds from yolk sac endothelium from E8.25 onwards [10, 11, 14, 17]. These cells leave the yolk sac via the circulation to colonise the liver [14, 18], where they expand into monocytes that subsequently colonise peripheral organs to differentiate into tissue-resident macrophages, thereby diluting the pool of early EMP-derived macrophages in many organs but not the CNS [10, 16].

Lineage tracing with *Csf1r-iCre* identifies ECs in developing brain vasculature

To target early EMPs [10, 13, 15], microglia [19, 20] and other differentiated MCs [21], we and others have used a transgene that expresses CRE recombinase under the control of the promoter for the myeloid lineage gene *Csf1r* (*Fms*), which encodes the colony-stimulating factor 1 receptor CSF1R. Microglia appear as amoeboid or ramified single YFP^+ cells in hindbrains from mouse embryos carrying *Csf1r-iCre* and the $Rosa^{Yfp}$ CRE/*LoxP* recombination reporter, with microglia and ECs also stained for isolectin B4 (IB4) (**Fig. 1a**) [19]. As previously shown [4], the number of $IB4^+YFP^+$ microglia in the hindbrain subventricular zone increased between E10.5 and E11.5, when vessels fuse into the subventricular vascular plexus (SVP), and decreased after SVP formation by E12.5, when they move into deeper hindbrain layers (**Fig. 1b**). Surprisingly, *Csf1r-iCre* additionally targeted sporadic elongated $IB4^+$ cells that appeared bound into the endothelium and increased in number between E10.5 and E12.5 alongside SVP expansion (**Fig. 1a-c; Extended Data Fig. 1a**). *Csf1r-iCre*-targeting of vessel-bound cells was not an artefact caused by spontaneous recombination of the

Rosa^{Yfp} reporter or unspecific immunostaining, because *Rosa*^{Yfp} littermates lacking *Csf1r-iCre* also lacked YFP staining (**Fig. 1a**). Furthermore, immunostaining of *Csf1r-iCre* hindbrains carrying *CAG-Cat-Egfp* as an alternative recombination reporter or imaging of tdTomato (tdTom) fluorescence in *Csf1r-iCre* hindbrains with the *Rosa*^{tdTom} reporter confirmed targeting of both microglia and vessel-bound elongated cells (**Extended Data Fig. 1b,c**). The independently generated *Csf1r-Mer-iCre-Mer* transgene, in which tamoxifen treatment is required for CRE activation [22], also targeted both vessel-bound cells and microglia in E12.5 hindbrains (**Fig. 1d**).

Immunolabelling of E12.5 *Csf1r-iCre;Rosa*^{Yfp} hindbrains for YFP and the macrophage marker F4/80 (ADGRE1) or the pericyte marker NG2 excluded that vessel-bound YFP$^+$ cells were microglia/perivascular macrophages or pericytes (**Extended Data Fig. 1d,e**). Instead, immunolabelling for the EC-specific transcription factor ERG and surface marker PECAM1 (CD31) showed that vessel-bound, elongated *Csf1r-iCre*-targeted cells were ECs (**Fig. 1e)**. Accordingly, their morphology was similar to ECs targeted with CRE encoded by the *Cdh5-Cre*^{ERT2} transgene, which is expressed in ECs but not microglia [23] and was activated by low dose tamoxifen treatment (**Fig. 1e**). Moreover, *Csf1r-iCre*-targeted ECs formed CDH5$^+$ junctions with neighbouring non-targeted ECs (**Extended Data Fig. 1f**).

Immunolabelling of E11.5 *Csf1r-iCre;Rosa*^{Yfp} hindbrains showed that microglia were CSF1R$^+$ YFP$^+$, as expected, but neither YFP$^-$ nor YFP$^+$ ECs expressed the CSF1R protein (**Extended Data Fig. 2a**). To determine whether the *Csf1r* promoter is active in ECs despite their lack of CSF1R protein expression, we used a *Csf1r-Egfp* transgene that faithfully reports *Csf1r* promoter activity as EGFP expression [24, 25]. However, unlike microglia, ECs were not EGFP$^+$ (**Extended Data Fig. 2b**). Further, the analysis of publicly available transcriptomic datasets [26] showed that *Csf1r* is neither expressed in E14.5 brain nor liver or lung ECs (**Extended Data Fig. 2c**). Finally, fluorescence-activated cell sorting (FACS) of *Csf1r-iCre*-lineage traced (tdTom$^+$) ECs and MCs with antibodies for PECAM1 versus the pan-hematopoietic marker CD45 (PTPRC) showed that tdTom$^+$ PECAM1$^-$ CD45$^+$ MCs expressed *Csf1r*, whereas tdTom$^+$ PECAM1$^+$ CD45$^-$ ECs expressed *Cdh5*, but not the the myeloid marker *Spi1* (*Pu.1*) or *Csf1r* (**Extended Data Fig. 2d-g**). Putative *Csf1r* expression by a subset of brain ECs therefore does not explain *Csf1r-iCre*-mediated endothelial targeting.

Csf1r-iCre-targeted ECs and EMPs are PU.1-independent and share spatiotemporal origins

Lack of endothelial CSF1R expression suggests that *Csf1r-iCre*-targeted brain ECs arise from precursors that activate *Csf1r* prior to their incorporation into hindbrain vasculature. By examining *Csf1r-iCre;Rosa*^{Yfp} hindbrains from *Pu.1* (*Spi1)*-null mice, we excluded that *Csf1r-iCre*-targeted ECs were derived from differentiated MCs or the recently identified tissue-resident myeloid precursors of pericytes [4, 23]. Thus, we found that PU.1 deficiency prevented the formation of YFP$^+$ F4/80$^+$ IB4$^+$ microglia, as expected, but did not reduce the number of YFP$^+$ IB4$^+$ F4/80$^-$ ECs (**Fig. 1f-h)**. Microglia were also absent from the striatum of *Csf1r-iCre;Rosa*^{Yfp}*;Pu.1*$^{-/-}$ brains on postnatal

day (P) 0, although YFP$^+$ ECs were present (**Extended Data Fig. 2h)**.

As PU.1 is not required for EMP formation [27], we investigated whether the formation of *Csf1r-iCre*-targeted ECs is mechanistically linked to the emergence of *Csf1r*$^+$ EMPs. E8.5 *Csf1r-Egfp* yolk sacs contained clusters of round EGFP$^+$ VEGFR2$^+$ cells that protruded from VEGFR2$^+$ endothelium into the vascular lumen (**Fig. 2a**), consistent with previously described EMP budding [14] and prior work showing that EMPs express *Csf1r* [10] and *Vegfr2* [12]. *Csf1r-iCre* lineage tracing similarly identified round VEGFR2$^+$ cells that protruded into the yolk sac vascular lumen (**Fig. 2b**), including round cells that expressed the EMP marker KIT [10] and persisted in PU.1-deficient yolk sacs at E8.5 **(Fig. 2c; Extended Data Fig. 3a,b)**. The endothelium of vessels in *Csf1r-iCre;Rosa*^{Yfp} yolk sacs additionally contained larger and flatter YFP$^+$ VEGFR2$^+$ cells, which lacked active *Csf1r* expression (compare **Fig. 2a** with **2b**). These cells also lacked KIT, but were PU.1-independent (**Fig. 2c; Extended Data Fig. 3b**), similar to *Csf1r-iCre*-targeted hindbrain ECs.

Tamoxifen-induced, CRE-mediated reporter recombination is highest approximately 6 h after and ends 24 h after injecting a single tamoxifen dose into a pregnant dam [28], allowing us to activate *Csf1r-Mer-iCre-Mer;Rosa*^{tdTom} in discrete temporal windows at E8.5, E9.5 or E10.5 before identifying lineage-traced cells in E12.5 yolk sacs by immunostaining (**Extended Data Fig. 3c**). Yolk sac macrophages were labelled after E8.5 induction (**Extended Data Fig. 3d**), consistent with their origin from early *Csf1r*$^+$ EMPs [10]. Induction at E9.5 or E10.5 also labelled yolk sac macrophages, likely because macrophages express *Csf1r* from E9.5 onwards [13, 15]. Induction at E8.5 or E9.5 additionally yielded tdTom$^+$ yolk sac ECs, whereas induction at E10.5 did not (**Extended Data Fig. 3d**). As EMPs are present in the yolk sac at E8.5 and E9.5, but home to the liver thereafter [16], their local availability makes them plausible precursors of *Csf1r-iCre*-labelled yolk sac ECs. In agreement, tamoxifen induction of a *Kit*^{CreERT2} knockin allele [29] at E8.5, when KIT$^+$ EMPs are in the yolk sac [14], labelled VEGFR2$^+$ ERG$^+$ yolk sac ECs alongside macrophages (**Extended Data Fig. 3e,f**).

A recent study showed that late wave EMPs lack *Csf1r* expression when they form [10]. To investigate whether these EMPs express *Csf1r* after their liver homing, we paired *Csf1r-Mer-iCre-Mer;Rosa*^{tdTom} with *Csf1r-Egfp* mice and induced pregnant dams with tamoxifen at E10.5 before analysing E11.5 liver cells via FACS to distinguish differentiated MCs and EMPs [10, 13, 14]. We observed tdTom$^+$ *Csf1r-Egfp*$^+$ cells in the KIT$^-$ CD45$^+$ differentiated MC population, as expected, but also in the KIT$^+$ CD45^{lo} progenitor population that includes EMPs (**Fig. 3a,b; Extended Data Fig. 3g-l**; KIT$^+$ CD45$^-$ cells were neither MCs nor EMPs, because they lacked CD45, tdTom and EGFP). Blood cell analysis showed that cells from the *Csf1r-Egfp*$^+$ tdTom$^+$ KIT$^+$ CD45^{lo} population that includes EMPs was still circulating at E11.5 and therefore could access embryonic organ vasculature (**Fig. 3a,b**).

To investigate whether *Csf1r* expression by late wave intraembryonic EMPs correlated with the emergence of *Csf1r-iCre*-targeted hindbrain ECs, we induced *Csf1r-Mer-iCre-Mer;Rosa*^{tdTom}

embryos at E8.5, E9.5 or E10.5 and visualised tdTom expression in E12.5 hindbrains (**Fig. 3c**). Microglia were targeted at all three stages, consistent with their origin from early *Csf1r*-expressing EMPs and their active *Csf1r* expression; in contrast, hindbrain vasculature contained tdTom$^+$ ECs following induction at E10.5, but not E8.5 or E9.5 (**Fig. 3d**). Accordingly, intraembryonic *Csf1r-iCre*-targeted ECs emerge at a time when late wave EMPs have moved from the yolk sac into the embryo proper and have activated *Csf1r* expression [10]. *Kit^{CreERT2}* induction at E8.5, when both early and late KIT$^+$ EMPs are present in the yolk sac, caused microglia targeting (**Fig. 3e,f**), suggesting that microglia can still be generated around E8.5 from KIT$^+$ progenitor-derived yolk sac macrophages [11]. This approach also yielded tdTom$^+$ ECs in the E12.5 hindbrain and therefore corroborated that yolk sac-born EMPs can give rise to intraembryonic ECs. Lineage tracing from three independent *Cre* alleles therefore suggests that EMPs can differentiate into ECs.

The *Csf1r-iCre*-targeted EMP lineage gives rise to ECs *in vitro*

The myeloid and erythroid potential of EMPs has been demonstrated through *in vitro* differentiation assays [14, 30]. To investigate their endothelial potential, we FACS-isolated KIT$^-$ CD45$^+$ PECAM1$^-$ differentiated MCs and the KIT$^+$ CD45^{lo} PECAM1$^-$ population that contains EMPs from E12.5 *Csf1r-iCre;Rosa^{tdTom}* liver and blood, and then used these cell populations for *in vitro* differentiation that were combined with immunolabelling for myeloid and EC markers. Both populations were mostly tdTom$^+$ (**Fig. 4a,b**). As expected [10], the EMP population was comprised of large round cells with a large nucleus and little cytoplasm, whereas the MC population contained granulocytes as well as monocytes in the liver and macrophages in the blood (**Fig. 4a,b**). We next cultured both cell populations in methocult, which promotes the formation of hematopoietic colonies, but additionally included a fibronectin substrate to facilitate EC differentiation. The differentiated tdTom$^+$ MCs from both the liver and blood persisted as single round/amoeboid cells (**Fig. 4c,d**) that were ERG^{lo} VEGFR2^{lo} (**Fig. 4e,f**; secondary antibody only controls in **Extended Data Fig. 4a,b**). In contrast, the tdTom$^+$ EMP populations from both the liver and blood formed myeloid and erythroid cell colonies in suspension (**Fig. 4c,d**). Moreover, both the EMP populations gave rise to single adherent cells, which resembled ECs due to their spindle-shaped/elongated morphology, lacked myeloid cell markers and were ERG^{hi} VEGFR2^{hi}, consistent with an EC identity (**Fig. 4e,f**; **Extended Data Fig. 4b,c**). In contrast, most neighbouring, adherent round/amoeboid cells expressed markers indicative of MC differentiation, including CD45, F4/80 or CSF1R (**Fig. 4e,f**; **Extended Data Fig. 4c**). Together, these experiments demonstrate that EMPs have endothelial potential alongside their known hematopoietic capacity.

***Csf1r-iCre*-targeted ECs support the growth of embryonic brain vasculature**

Hoxa cluster genes regulate haematopoiesis [31] and are upregulated in postnatal compared to adult ECs [32], with HOXA9 also shown to promote EC differentiation from progenitor cells in adult

ischemic disease [33]. Our analysis of published transcriptomic data [12, 34] revealed that several *Hoxa* transcripts are enriched in E10.25 compared to E9.0 EMPs or differentiated macrophages (**Fig. 5a**). To investigate whether *Hoxa*-deficiency impaired the formation of EMP-derived ECs, we crossed *Csf1r-iCre* and *Rosa*^{tdTom} into mice carrying a conditional null *Hoxa* cluster mutation (*Hoxa*^{fl}) [35] (**Extended Data Fig. 5a**). Gene copy analysis showed effective gene targeting in KIT$^+$ cells from E12.5 *Csf1r-iCre;Hoxa*$^{fl/fl}$ mutant compared to control livers, but the number of CD45$^+$ cells, including differentiated MCs, was not reduced (**Extended data Fig. 5b-f**). These findings suggest that *Hoxa* genes are dispensable for MC specification from late wave EMPs. In contrast, significantly fewer tdTom$^+$ ECs, also derived from late wave EMPs, had formed in *Csf1r-iCre;Rosa*^{tdTom}*;Hoxa*$^{fl/fl}$ mutant compared to control hindbrains; moreover, SVP complexity was significantly reduced in the mutant compared to control hindbrains **(Fig. 5b-d**). Although we also observed 20% fewer microglia in mutant compared to control hindbrains (**Extended data Fig. 5g-i**), this unlikely contributed to the vascular defect, because even 50% fewer microglia in *Csf1*$^{op/+}$ mutants did not reduce SVP complexity (**Extended data Fig. 5j-l**). Together, these findings suggest that *Hoxa* cluster genes promote the formation of EMP-derived brain ECs, which in turn support normal brain vascular development.

The EMP-derived EC population has a core endothelial transcriptional signature with enrichment for liver EC markers

As *Csf1r-iCre*-targeted ECs appeared morphologically similar to neighbouring ECs (e.g. **Fig. 1**), with similarly slow proliferation and overall cell cycle kinetics (**Extended Data Fig. 6**), we next compared the gene expression signature of both EC types by RNAseq. Thus, we used E12.5 *Csf1r-iCre;Rosa*^{tdTom} embryos for FACS to separate tdTom$^+$ and tdTom$^-$ ECs, defined as PECAM1$^+$ cells lacking KIT, CD45 and CD11b (ITGAM) (**Fig. 6a**). Both EC populations differed by their expression of the *Rosa* transcript, as expected (**Extended Data Fig. 7a**), but otherwise had largely similar transcriptomes with few differentially expressed genes (**Fig. 6b**,**c**). Consistent with an endothelial identity, tdTom$^+$ ECs lacked markers for differentiated MCs and other non-EC lineages, but expressed transcripts for core EC markers at similar levels as tdTom$^-$ ECs (**Fig. 6d,e**). Amongst the differentially expressed genes, markers typical of EC specialisation were under-represented in tdTom$^+$ ECs, such as ephrins and their EPH receptors, which regulate arteriovenous differentiation, or *Slc2a1*, a marker of brain EC maturation (**Fig. 6c,e,f**). Reverse transcriptase quantitative PCR (RT-qPCR) comparisons confirmed that the brain EC maturation marker *Slc2a1* was expressed at lower levels in tdTom$^+$ than tdTom$^-$ ECs at E12.5, consistent with delayed endothelial differentiation (**Extended data Fig. 7b**). This observation agrees with the idea that *Csf1r-iCre* lineage-traced ECs in the brain are derived from circulating progenitors that are recruited into a vascular endothelium that is pre-formed by ECs of classical origin. Whereas *Slc2a1* and other markers of brain ECs were under-represented in the embryo-wide tdTom$^+$ EC

population, liver EC markers were over-represented (e.g. *Oit3, Mrc1*), including early markers of liver sinusoidal differentiation (*Stab2* and *Lyve1*) [36] (**Fig. 6c,f**)**.** These observations were confirmed by RT-qPCR (**Extended data Fig. 7b,c**). RT-qPCR confirmed that liver transcripts were expressed at similar levels in tdTom$^+$ and tdTom$^-$ liver ECs (**Extended Data Fig. 7d**), thereby corroborating that EMP- and non-EMP-derived ECs are overall similar. Moreover, this finding suggested that the over-representation of liver EC transcripts in the total embryonic EC population reflected a preferential contribution of EMP-derived vascular progenitors to liver vasculature rather than altered liver EC differentiation. Immunostaining and flow cytometry of *Csf1r-iCre;Rosa*^{tdTom} E12.5 and E18.5 embryos confirmed that tdTom$^+$ ECs were more prevalent in liver endothelium than tdTom$^-$ ECs (**Fig. 6g,i**; **Extended Data Figs. 8 and 9a,b**). Agreeing with the RT-qPCR analysis, MRC1 as well as LYVE1 were observed in both tdTom$^-$ and tdTom$^+$ ECs within E12.5 liver vasculature (**Fig. 6g**; **Extended Data Fig. 8a**). Liver ECs of two distinct origins therefore undergo similar organ-specific EC differentiation.

***Csf1r-iCre*-targeted ECs populate multiple embryonic organs and persist into adulthood**

Immunostaining and FACS analyses at E18.5 confirmed that *Csf1r-iCre*-targeted ECs contribute to brain and liver, but also heart and lung vasculature (**Fig. 6i**; **Extended Data Fig. 8 and 9a,b**). EMPs therefore contribute to organ vasculature at multiple sites (working model in **Extended Data Fig. 9c**). Corresponding immunostaining and FACS analyses of adult organs showed that tdTom$^+$ ECs persisted in the brain, heart, lung and liver (**Fig. 6h,j; Extended Data Fig. 10**). Moreover, tdTom$^+$ ECs continued to dominate the LYVE1$^+$ MRC1$^+$ liver sinusoidal endothelium of adult mice (**Fig. 6h,j**; **Extended Data Fig. 10b**). Accordingly, organs differ with respect to their content of EMP-derived ECs, with a remarkably high contribution to liver sinusoidal endothelium in both embryos and adults.

Discussion

The heterogeneous origin of blood vascular mural cells from distinct populations of mesodermal progenitors, hematopoietic and neural crest cells is established [37]. Here, we have combined constitutive and temporally inducible lineage tracing with FACS, immunostaining, transcriptomic analyses and cell culture assays to show that embryonic vascular endothelium has two major origins: a classical origin via angioblast differentiation into ECs and the unexpected differentiation of ECs from the EMP lineage. Multiple prior investigations have utilised the *Csf1r-iCre* transgene together with recombination reporters to follow the embryonic myeloid lineage [10, 13, 15]. These studies predominantly employed flow cytometry with hematopoietic markers, which precluded the observation of *Csf1r-iCre*-targeted ECs. In contrast, we included EC markers to isolate *Csf1r-iCre*-targeted ECs alongside MCs from embryonic and adult organs. Immunostaining of tissues was

previously also used to identify *Csf1r-iCre*-targeted cells in the retina [20], liver and colon [21], but without description of EC targeting, possibly because of the close spatial proximity of ECs and perivascular macrophages [4, 6]. By performing high resolution imaging after immunostaining for EC and macrophage makers, we have overcome this limitation to demonstrate targeting of both cell types alongside each other *in situ*. The contribution of EMP-derived ECs to yolk sac, brain, heart and lung vasculature is proportionally smaller than that of ECs of classical origin, whereas EMP-derived ECs predominate the liver, particularly the sinusoidal endothelium. Liver endothelium was previously reported to be heterogeneous in origin, with an endoderm lineage contribution of approximately 15% and the remainder of the liver EC population attributed to a venous origin, i.e. angiogenic ingrowth from nearby veins [38]. Our results suggest that liver endothelium additionally contains approximately 60% EMP-derived ECs, accordingly decreasing prior estimates for liver ECs of venous origin. Preferential EMP homing to the liver after their entry into the embryonic circulation [16] and the dependence of liver growth on rapid vascular expansion [39] may explain the relatively large contribution of EMP-derived ECs to this organ. Ultimately, the discovery that EMPs provide a source of ECs for organ vasculature may open up new therapeutic avenues for vessel-dependent organ repair and regeneration. For example, EMPs or EMP-like EC progenitors, derived from human stem cells via genetic manipulation of factors such as or including *Hoxa* genes, may be delivered systemically to support vascular growth in ischemic diseases or provide angiocrine signals that stimulate tissue stem cells.

References

1. Potente, M., Gerhardt, H. & Carmeliet, P. Basic and therapeutic aspects of angiogenesis. *Cell* **146**, 873-887 (2011).
2. Hirschi, K.K., Ingram, D.A. & Yoder, M.C. Assessing identity, phenotype, and fate of endothelial progenitor cells. *Arteriosclerosis, thrombosis, and vascular biology* **28**, 1584-1595 (2008).
3. Pollard, J.W. Trophic macrophages in development and disease. *Nature Reviews Immunology* **9**, 259-270 (2009).
4. Fantin, A. *et al.* Tissue macrophages act as cellular chaperones for vascular anastomosis downstream of VEGF-mediated endothelial tip cell induction. *Blood* **116**, 829-840 (2010).
5. Gerri, C. *et al.* Hif-1alpha regulates macrophage-endothelial interactions during blood vessel development in zebrafish. *Nat Comm* **8**, 15492 (2017).
6. Liu, C. *et al.* Macrophages Mediate the Repair of Brain Vascular Rupture through Direct Physical Adhesion and Mechanical Traction. *Immunity* **44**, 1162-1176 (2016).
7. Cattin, A.L. *et al.* Macrophage-Induced Blood Vessels Guide Schwann Cell-Mediated Regeneration of Peripheral Nerves. *Cell* **162**, 1127-1139 (2015).

8. Clausen, B.E., Burkhardt, C., Reith, W., Renkawitz, R. & Forster, I. Conditional gene targeting in macrophages and granulocytes using LysMcre mice. *Transgenic research* **8**, 265-277 (1999).
9. de Boer, J. *et al.* Transgenic mice with hematopoietic and lymphoid specific expression of Cre. *European J Immuol* **33**, 314-325 (2003).
10. Hoeffel, G. *et al.* C-Myb(+) erythro-myeloid progenitor-derived fetal monocytes give rise to adult tissue-resident macrophages. *Immunity* **42**, 665-678 (2015).
11. Frame, J.M., McGrath, K.E. & Palis, J. Erythro-myeloid progenitors: "definitive" hematopoiesis in the conceptus prior to the emergence of hematopoietic stem cells. *Blood cells, molecules & diseases* **51**, 220-225 (2013).
12. Mass, E. *et al.* Specification of tissue-resident macrophages during organogenesis. *Science* **353** (2016).
13. Gomez Perdiguero, E. *et al.* Tissue-resident macrophages originate from yolk-sac-derived erythro-myeloid progenitors. *Nature* **518**, 547-551 (2015).
14. McGrath, K.E. *et al.* Distinct Sources of Hematopoietic Progenitors Emerge before HSCs and Provide Functional Blood Cells in the Mammalian Embryo. *Cell Reports* **11**, 1892-1904 (2015).
15. Schulz, C. *et al.* A lineage of myeloid cells independent of Myb and hematopoietic stem cells. *Science* **336**, 86-90 (2012).
16. Ginhoux, F. & Guilliams, M. Tissue-Resident Macrophage Ontogeny and Homeostasis. *Immunity* **44**, 439-449 (2016).
17. Hoeffel, G. & Ginhoux, F. Fetal monocytes and the origins of tissue-resident macrophages. *Cell Immunol* (2018). doiL 10.1016/j.cellimm.2018.01.001 [Epub ahead of print]
18. Lux, C.T. *et al.* All primitive and definitive hematopoietic progenitor cells emerging before E10 in the mouse embryo are products of the yolk sac. *Blood* **111**, 3435-3438 (2008).
19. Fantin, A. *et al.* NRP1 acts cell autonomously in endothelium to promote tip cell function during sprouting angiogenesis. *Blood* **121**, 2352-2362 (2013).
20. Stefater, J.A., 3rd *et al.* Regulation of angiogenesis by a non-canonical Wnt-Flt1 pathway in myeloid cells. *Nature* **474**, 511-515 (2011).
21. Deng, L. *et al.* A novel mouse model of inflammatory bowel disease links mammalian target of rapamycin-dependent hyperproliferation of colonic epithelium to inflammation-associated tumorigenesis. *Am J Pathol* **176**, 952-967 (2010).
22. Qian, B.Z. *et al.* CCL2 recruits inflammatory monocytes to facilitate breast-tumour metastasis. *Nature* **475**, 222-225 (2011).
23. Yamazaki, T. *et al.* Tissue Myeloid Progenitors Differentiate into Pericytes through TGF-beta Signaling in Developing Skin Vasculature. *Cell Reports* **18**, 2991-3004 (2017).
24. Sasmono, R.T. *et al.* A macrophage colony-stimulating factor receptor-green fluorescent protein transgene is expressed throughout the mononuclear phagocyte system of the mouse. *Blood* **101**, 1155-1163 (2003).

25. Burnett, S.H. *et al.* Conditional macrophage ablation in transgenic mice expressing a Fas-based suicide gene. *J Leukocyte Biol* **75**, 612-623 (2004).
26. Tam, S.J. *et al.* Death receptors DR6 and TROY regulate brain vascular development. *Dev Cell* **22**, 403-417 (2012).
27. Kierdorf, K. *et al.* Microglia emerge from erythromyeloid precursors via Pu.1- and Irf8-dependent pathways. *Nature Neuroscience* **16**, 273-280 (2013).
28. Wilson, C.H. *et al.* The kinetics of ER fusion protein activation in vivo. *Oncogene* **33**, 4877-4880 (2014).
29. Klein, S. *et al.* Interstitial cells of Cajal integrate excitatory and inhibitory neurotransmission with intestinal slow-wave activity. *Nat Comm* **4**, 1630 (2013).
30. Palis, J., Robertson, S., Kennedy, M., Wall, C. & Keller, G. Development of erythroid and myeloid progenitors in the yolk sac and embryo proper of the mouse. *Development* **126**, 5073-5084 (1999).
31. Alharbi, R.A., Pettengell, R., Pandha, H.S. & Morgan, R. The role of HOX genes in normal hematopoiesis and acute leukemia. *Leukemia* **27**, 1000-1008 (2013).
32. Toshner, M. *et al.* Transcript analysis reveals a specific HOX signature associated with positional identity of human endothelial cells. *PloS one* **9**, e91334 (2014).
33. Rossig, L. *et al.* Histone deacetylase activity is essential for the expression of HoxA9 and for endothelial commitment of progenitor cells. *J Exp Med* **201**, 1825-1835 (2005).
34. Browning, A.C. *et al.* Comparative gene expression profiling of human umbilical vein endothelial cells and ocular vascular endothelial cells. *Br J Ophthalmol* **96**, 128-132 (2012).
35. Kmita, M. *et al.* Early developmental arrest of mammalian limbs lacking HoxA/HoxD gene function. *Nature* **435**, 1113-1116 (2005).
36. Nonaka, H., Tanaka, M., Suzuki, K. & Miyajima, A. Development of murine hepatic sinusoidal endothelial cells characterized by the expression of hyaluronan receptors. *Dev Dyn* **236**, 2258-2267 (2007).
37. Majesky, M.W. Developmental basis of vascular smooth muscle diversity. *Arteriosclerosis, thrombosis, and vascular biology* **27**, 1248-1258 (2007).
38. Goldman, O. *et al.* Endoderm generates endothelial cells during liver development. *Stem Cell Reports* **3**, 556-565 (2014).
39. Matsumoto, K., Yoshitomi, H., Rossant, J. & Zaret, K.S. Liver organogenesis promoted by endothelial cells prior to vascular function. *Science* **294**, 559-563 (2001).

Supplementary information is available in the online version of the paper.

Acknowledgements

We thank the Biological Resources, FACS, Imaging and Genomics facilities at UCL and E. Scarpa for technical help, D. Saur, A. Mass, D. Duboule, M. Kmita and Y. Kubota for mouse strains, M.

Golding for helpful discussions. This research was supported by grants from the Wellcome Trust (095623/Z/11/Z, 101067/Z/13/Z), Medical Research Council (MR/N011511/1) and British Heart Foundation (FS/17/23/32718).

Author contributions

A.P., A.F. and C.R. conceived and planned this study, analysed the data and co-wrote the manuscript. L.D. performed genetic crosses and genotyping. A.P. and A.F. performed experiments either together or replicated each other's experiments, except for the cell cycle and *Hoxa* studies, which were carried out by A.P and A.F., respectively. J.W.P. provided mouse strains. C.R. supervised the project. All authors reviewed and edited the manuscript.

Author information. Reprints and permission information is available at www.nature.com/reprints. The authors declare no competing interests. Correspondence and requests for materials should be addressed to C.R. (c.ruhrberg@ucl.ac.uk).

Data availability. All sequence data used in this study have been deposited in the NCBI Gene Expression Omnibus database and are accessible through accession numbers GSExxxx.

Figure legends

Fig. 1: *Csf1r-iCre* lineage tracing identifies ECs in developing brain vasculature.

(**a**) Confocal z-stacks of hindbrains of the indicated genotypes and gestational stages, wholemount labelled for YFP and IB4, identified *Csf1r-iCre* targeting of vessel-bound cells during hindbrain vascularisation. (**b**) Number of YFP^+ $IB4^+$ single cells (microglia) and YFP^+ $IB4^+$ vessel-bound cells (putative ECs) per 0.72 mm^2; mean ± SD, n=3 hindbrains each. (**c**) Correlation between vessel area and number of YFP^+ putative ECs; r^2, coefficient of determination; $P < 0.01$; each data point represents the value of one hindbrain.

(**d**) Confocal z-stack of an E12.5 *Csf1r-Mer-iCre-Mer;*$Rosa^{tdTom}$ hindbrain after tamoxifen delivery on E10.5, IB4 wholemount labelled and shown including tdTom fluorescence.

(**e**) Confocal z-stacks of *Csf1r-iCre;*$Rosa^{tdTom}$ and *Cdh5-*Cre^{ERT2}*;*$Rosa^{tdTom}$ E12.5 hindbrains, wholemount labelled for the endothelial markers ERG and PECAM1 and shown including tdTom fluorescence to demonstrate that *Csf1r-iCre* targets ECs; *Cdh5-*Cre^{ERT2} was induced with a low tamoxifen dose at E11.5.

(**f-h**) Confocal z-stacks of *Csf1r-iCre;*$Rosa^{Yfp}$ E11.5 hindbrains on a $Pu.1^{+/+}$ versus $Pu.1^{-/-}$

background, wholemount labelled for YFP and F4/80 together with IB4, show that *Csf1r-iCre*-targeted ECs are PU.1-independent. The boxed area in (**f**) was 3D surface rendered and is shown in (**g**) en face and as a lateral view starting at the plane indicated by the yellow line; the stippled line outlines the vascular lumen (lu). (**h**) Quantification of YFP^+ microglia (*Pu.1*$^{+/+}$ n=4; *Pu.1*$^{-/-}$ n=3) and ECs (*Pu.1*$^{+/+}$ n=6; *Pu.1*$^{-/-}$ n=7); mean ± SD; each data point represents the value for one hindbrain; n.s., non-significant, * P > 0.05 (unpaired t-test).

Symbols: Microglia and ECs are indicated with arrowheads and arrows, respectively. Solid and clear symbols indicate the presence or absence of marker expression, respectively.

Scale bars: 20 µm (**a,d,f**), 50 µm (**e**).

Fig. 2: *Csf1r-iCre*-targeted ECs emerge concomitantly with EMPs in the yolk sac.

Confocal z-stacks of E8.5 yolk sacs from *Csf1r-Egfp* mice (**a**) or *Csf1r-iCre;Rosa*^{Yfp} mice on a *Pu.1*$^{+/+}$ *versus Pu.1*$^{-/-}$ background (**b**), wholemount labelled for VEGFR2 and EGFP (**a**) or YFP (**b**). Lateral views of 3D-rendered yolk sac vasculature starting at the positions indicated by cyan and orange lines show lineage-traced YFP^+ $VEGFR2^+$ flat cells in the vascular wall and $VEGFR2^+$ round cells expressing EGFP or YFP, respectively, protruding from the vascular wall into the lumen (lu). *Symbols*: Wavy arrows indicate $EGFP^+$ or YFP^+ $VEGFR2^+$ EMPs/MPs, straight arrows YFP^+ $VEGFR2^+$ ECs. *Scale bars*: 20 µm.

Fig. 3: *Csf1r-iCre-targeted hindbrain ECs emerge from intraembryonic EMPs*.

(**a,b**) A pregnant *Csf1r-Egfp*;*Csf1r-Mer-iCre-Mer;Rosa*^{tdTom} dam was injected with a single tamoxifen dose on E10.5 (**a**) before E11.5 liver and blood cells were analysed by flow cytometry (**b**) for CD45 and KIT, followed by gating the $CD45^{hi}$ KIT^- differentiated MC (blue) and $CD45^{lo}$ KIT^+ EMP/myeloid progenitor (MP) populations (pink) for EGFP and tdTom (n=4 embryos).

(c-f) Pregnant *Csf1r-Mer-iCre-Mer;Rosa*^{tdTom} (**c,d**) and *Kit*$^{CreERT2;}$*Rosa*^{tdTom} (**e,f**) dams were injected with a single tamoxifen dose on the indicated days and confocal z-stacks obtained of E12.5 hindbrains after wholemount staining for the indicated markers, shown including tdTom fluorescence. *Symbols*: Arrows indicate $tdTom^+$ ECs, arrowheads macrophages and microglia and wavy arrows a cluster of $tdTom^+$ ERG^- $IB4^-$ neural progenitors, which express *Kit* at E8.5. *Scale bars*: 20 µm.

Fig. 4: EMPs in the liver and blood give rise to ECs *in vitro*.

(**a,b**) FACS gating strategy for separation of the indicated cell populations, including EMP lineage cells, from E12.5 *Csf1r-iCre;Rosa*^{tdTom} liver (**a**) and blood (**b**) using antibodies for PECAM1, CD45 and KIT (top), including proportion of cells with tdTom recombination in the MC and EMP/MP

populations and Giemsa-Wright staining of representative cells (bottom); Mo, monocyte; GC, granulocyte; MΦ, macrophage.

(**c,d**) Brightfield images of hematopoietic colonies formed after three days in methocult (met.); note white and reddish colour of myeloid and erythroid colonies, respectively. (**e,f**) Fibronectin (FN)-adherent cells after three days in methocult were immunolabelled for the EC markers ERG and VEGFR2 and counterstained with the nuclear label DAPI. *Symbols*: Arrows indicate tdTom$^+$ ECs, arrowheads tdTom$^+$ MCs. Solid and clear symbols indicate high versus low level expression, respectively, of the indicated markers. *Scale bars*: 20 µm.

Fig. 5: *Csf1r-iCre*-targeted ECs form in a *Hoxa*-dependent mechanism and promote vascularisation in the embryonic hindbrain.

(**a**) Transcriptomic analysis of the indicated cell populations, based on published RNAseq and EC microarray data [12, 34] (n ≥ 2), shows that *Hoxa* genes are enriched in intraembryonic EMPs; white represents low and black high relative expression levels of the indicated genes.

(**b**) Confocal z-stacks of E12.5 littermate hindbrains of the indicated genotypes, wholemount labelled for F4/80, RFP to visualise tdTom and with IB4. *Symbols*: Arrows and arrowheads indicate tdTom$^+$ ECs and microglia, respectively. *Scale bars*: 50 µm.

(**c**) Percentage of tdTom$^+$ relative to IB4$^+$ EC volume in *Hoxa*$^{+/+}$ (n=3) versus *Hoxa*$^{fl/fl}$ mutant (n=7) hindbrains on a *Csf1r-iCre;Rosa*^{tdTom} background. (**d**) Number of vascular branchpoints in control (pooled *Csf1r-iCre*$^+$*;Hoxa*$^{+/+}$ and *Csf1r-iCre*$^-$ of any *Hoxa* genotype; n=13) versus *Hoxa*$^{fl/fl}$*;Csf1r-iCre* mutant (n=9) hindbrains. Mean ± SD fold change; each data point represents the value for one hindbrain; * P < 0.05 (unpaired t-test).

Fig. 6: *Csf1r-iCre*-targeted ECs have a core endothelial transcription signature with an increase in liver EC transcripts, and they persist in adult organ vasculature.

(**a**) FACS of PECAM1$^+$ CD45$^-$ CD11b$^-$ KIT$^-$ cells from E12.5 *Csf1r-iCre;Rosa*^{tdTom} embryos, including gating to separate tdTom$^-$ and tdTom$^+$ ECs for RNAseq. (**b**) Graphic representation of genes whose expression is significantly different (green dots) or similar (black dots) between both EC populations. (**c**) Volcano plot of 247 transcripts with on average > 100 counts that are significantly different between both populations; grey and red data points represent transcripts in tdTom$^-$ ECs with ≥2-fold over- or under-representation, respectively, with selected genes named. (**d-f**) Relative expression levels in both EC populations of (**d**) non-EC markers typical of myeloid (*Cx3cr1-Ptprc*), astrocytic (*Gfap*), smooth muscle (*Acta2*), neuronal (*Rbfox3*, *Nefl*), skeletal muscle (*Myog*) or epithelial (*Cdh1*) differentiation, (**e**) core EC or EC maturation markers and (**f**) representative brain or liver EC specialisation markers, shown alongside their relative expression in brain versus liver/lung ECs based on microarrays [31]. RNAseq analysis: mean of normalised

counts ± SD, n=3 samples each (DESeq2; Benjamini-Hochberg's multiple comparisons test for p-value adjustment, adjP). Microarray analysis: mean ± SD, n=5 samples each (2-way ANOVA, Bonferroni's multiple comparisons test). * P < 0.05, ** P < 0.01, *** P < 0.001, ns, non-significant.

(**g,h**) *Csf1r-iCre;Rosa*^{tdTom} E12.5 (**g**) and adult (**h**) liver cryosections were labelled for the indicated markers and RFP to visualise tdTom, including DAPI counterstaining in (**h**). *Symbols*: Arrows and arrowheads indicate tdTom^{+} ECs and macrophages, respectively. Clear arrowheads indicate VEGFR2^{-} macrophages. *Scale bar*: 50 μm.

(**i,j**) The relative contribution of tdTom^{+} ECs to organ vasculature at E12.5 (**i**) and in 12-week old adult mice (**j**) was determined by flow cytometry of *Csf1r-iCre;Rosa*^{tdTom} brain, heart, lung and liver. Mean ± SD; n ≥ 4 (E12.5) and n ≥ 6 (adult), with each data point representing an individual organ (1-way ANOVA, Tukey's multiple comparisons test, ** P < 0.01, *** P < 0.001).

(online only) Methods plus associated references

***Mouse strains*.** All animal procedures were performed in accordance with the institutional Animal Welfare Ethical Review Body (AWERB) and UK Home Office guidelines. To obtain mouse embryos of defined gestational age, mice were paired in the evening and the presence of a vaginal plug the following morning was defined as E0.5. In some studies, we analysed adult mice, defined as more than 8 weeks of age. Mice carrying the *Csf1r-iCre* transgene [21] were mated to *Rosa*^{Yfp} [40], *Rosa*^{tdTom} [41] or *CAG-cat-Egfp* [42] mice. PU.1 heterozygous null mice [43] were mated to *Rosa*^{Yfp} mice and then *Csf1r-iCre* mice to obtain *Csf1r-iCre;Rosa*^{Yfp}*;Pu.1*$^{-/-}$ embryos. *Hoxa*$^{fl/fl}$ mice [35] were mated to *Rosa*^{tdTom} mice and then *Csf1r-iCre* to obtain *Csf1r-iCre;Rosa*^{tdTom}*;Hoxa*$^{fl/fl}$ embryos. *Csf1r-Mer-iCre-Mer* [22], *Cdh5-Cre-ER*^{T2} [44] and *Kit*^{CreERT2} mice [29] were mated to *Rosa*^{tdTom} mice. We also used *Csf1r-Egfp-Ngfr/Fkbp1a/Tnfrsf6* (short: *Csf1r-Egfp*) mice as a reporter of *Csf1r* expression [25] and a loss of function mutation in *Csf1* (*Csf1*^{Op}) [45]. All mouse strains were maintained on a mixed background (C57Bl6/J;129/Sv), with the exception of *Csf1r-Mer-iCre-Mer*, which was maintained on a mixed FVB:C57/bl6 background. For tamoxifen induction of CRE activity, tamoxifen (Sigma) was dissolved to 2 mg/ml in peanut oil and administered via intraperitoneal injection into pregnant dams. For *Cdh5-Cre-ER*^{T2} and *Csf1r-Mer-iCre-Mer*, we injected 20 µg and 1 mg tamoxifen alone, respectively; for *Kit*$^{Cre-ERT2}$, we injected 3 mg tamoxifen together with 1.75 mg progesterone (Sigma).

***Immunolabelling*.** Samples were fixed in 4% formaldehyde in PBS and processed as either wholemount or 20 µm cryosections. Immunolabelling was performed as described previously [46] using the following antibodies and dilutions: goat anti-CDH5 (1:200; AF1002, lot FQI0116101, R&D Systems), rabbit anti-CSF1R (1:500; sc-692, lot K1212, Santa Cruz), rat anti-EMCN (1:50; sc-65495, lot C2917, Santa Cruz), rabbit anti-ERG (1:200; ab92513, lot GR32027 69-1, Abcam), rat anti-F4/80 (1:500; MCA497R, lot 1605, Serotec), chicken anti-GFP (1:1000; GFP-1020, lot 0511FP12, Aves) and rabbit anti-GFP (1:500; 598, lot 079, MBL) for YFP or EGFP labelling, rabbit anti-IBA1 (1:500; 019-19741, Wako Chemicals), rat anti-KIT (1:500; 553353, lot 30259, BD Pharmingen), rabbit anti-NG2 (1:200; AB5320, lot 2726769, Millipore), rat anti-PECAM1 (1:200; 553370, lot 5205656, BD Pharmingen), rabbit anti-pHH3 (1:400; 06-570, lot 2825969, Millipore), rabbit anti-RFP (1:1000; PM005, lot 045, MBL), goat anti-VEGFR2 (1:200; AF644, lot COA0417021, R&D Systems). Secondary antibodies used included Alexa Fluor-conjugated goat anti-chick, -rabbit or -rat IgG (Life Technologies), or, for primary antibodies raised in goat, donkey fluorophore-conjugated FAB fragments of anti-chick, -goat, -rabbit or -rat IgG (Jackson ImmunoResearch). Biotinylated IB4 (L2140, lot 085M4032V, Sigma) followed by Alexa-conjugated streptavidin (ThermoFisher) was used to detect brain endothelial cells and microglia [4, 19]. Nuclei were labelled with DAPI. Images were acquired with a LSM710 laser scanning confocal microscope (Zeiss) and processed using LSM image browser (Zeiss) and Photoshop CS4 (Adobe) software. Three-dimensional rendering including surface rendering and the generation of virtual

slices for lateral views of high-resolution confocal z-stacks was carried out with Imaris (Bitplane).

***Fluorescence-activated cells sorting (FACS) and cell culture*.** Tissues were mechanically and enzymatically homogenised in RPMI1640 with 2.5% foetal bovine serum (ThermoFisher), 100 µg/ml collagenase/dispase (Roche), 50 µg/ml DNAse (Qiagen) and 100 µg/ml heparin (Sigma), incubated for 5 mins with 0.5 mg/ml rat Fc block (Becton Dickinson) and labelled with a combination of PE/Cy7-conjugated rat anti-PECAM1 (clone 390, cat 102418, lot B212262), FITC-conjugated rat anti-CD45 (clone 30-F11, cat 103108, lot B246762) or CD41 (clone MWReg30, cat 133903, lot B201955), APC-conjugated rat anti-KIT (clone 2B8, cat 105812, lot B217855) and PerCp/Cy5.5-conjugated rat anti-CD11b (clone M1/70, cat 101227) (all Biolegend). Appropriate fluorescence gate parameters were established with unstained tissue, *Csf1r-iCre*- or *Csf1r-Egfp*-negative tissues and fluorescence-minus-one (FMO) staining. For cell cycle analysis, cell populations were incubated with 10 µg/ml Hoechst 33342 (Sigma) for 30 mins at 37˚C [47] before labelling with PE/Cy7-conjugated rat anti-PECAM1 and performing FACS analysis. In all experiments, doublets were eliminated using pulse geometry gates (FSC-H versus FSC-A and SSC-H versus SSC-A), whereas dead cells were removed using SYTOX Blue (Life Technologies) or LIVE/DEAD Fixable Violet (Life Technologies). Single cell suspensions were analysed using the BD LSRFortessa X-20 cell analyser or sorted using the BD Influx cell sorter (BD Biosciences); FlowJo software (FlowJo LLC) was used for subsequent analyses. In some experiments, a fraction of each population was cytospun onto a glass slide for Wright-Giemsa staining (Sigma) followed by imaging using an LSM510 microscope equipped with an AxioCam MRc camera (Zeiss). For cell culture experiments, cell populations were sorted into DMEM with 100 U/ml penicillin, 100 U/ml streptomycin and 20% foetal bovine serum (all ThermoFisher) before seeding the cells into a 96-well plate coated with 10 µg/ml fibronectin (ThermoFisher). Cells were cultured in methocult (Stemcell Technologies); haematopoietic colonies were imaged using a TS100 microscope equipped with a DS-5M colour camera (Nikon). Adherent cells were fixed with 4% formaldehyde in PBS and then labelled for VEGFR2, ERG, CD45, F4/80 and CSF1R (see above) before imaging using a Ti-E microscope (Nikon).

RNAseq. PECAM1$^+$ CD45$^-$ CD11b$^-$ KIT$^-$ ECs were isolated from E12.5 *Csf1r-Cre;Rosa*^{tdTom} embryos and divided into tdTom$^+$ and tdTom$^-$ populations with the Influx cell sorter before RNA was extracted with the RNeasy Micro Kit (QIAGEN). cDNA was generated and amplified using the SMART-seq V4 ultra low input RNA kit (Clontech). 100 pg of amplified cDNA per sample was used to prepare a library with the Nextera XT kit (Illumina) and run on the NextSeq 500 sequencer (Illumina). Raw sequence data were pre-processed to trim poor quality base calls and adapter contamination using Trimmomatic v.0.36.4 [48] and aligned to the mouse mm10 genome with STAR v.2.5.2b [49]. Mapped reads were deduplicated to reduce PCR bias using Picard v2.7.1.1 software (http://broadinstitute.github.io/picard/), and the reads-per-transcript were then calculated using FeatureCount v1.4.6.p5 software [50]. Differential expression was performed using the BioConductor package DESeq2 via the SARTools wrapper v1.3.2.0 [51].

Reverse transcription polymerase chain reaction (PCR). We isolated cells with the Influx cell sorter (see above). We extracted RNA with the RNeasy Micro Kit and synthesised cDNA with Superscript IV (ThermoFisher). Quantitative (q) RT-PCR was performed with SYBR Green on an HT7900 system (Applied Biosystems) using the following oligonucleotide pairs: *Actb* 5'-CACCACACCTTCTACAATGAG-3' and 5'-GTCTCAAACATGATCTGGGTC-3'; *Cdh5* 5'-GATGCAGATGACCCCACTGT-3' and 5'-AGGGCATCTTGTGTTCCAC-3'; *Csf1r* 5'-TGCGTCTACACAGTTCAGAG-3' and 5'-ATGCTGTATATGTTCTTCGGT-3'; *Spi1* 5'-GCCATAGCGATCACTACTG-3' and 5'-CAAGGTTTGATAAGGGAAGC-3'; *Hoxa11* 5'-TCTTTGCCTCTCTCCTTCCTT-3' and 5'-TTGCAGACGCTTCTCTTTGTT-3'; *Evx1* 5'-GTGTGCTCTGGGCTCCTGT-3' and 5'-GCCAGGGTGCCTTGAGAG-3; *Slc2a1* 5'-CCCCAGAAGGTTATTGAGGAGT and 5'-ACAAAGAGGCCGACAGAGAA; *Mrc1* 5'-ACTGGGCAATGCAAATGGAG and 5'- CCCTCAAAGTGCAATGGACA; *Oit3* 5'-CGTCTGCTTCCATGTCTACTG and 5'-GTGCTCACATTCATTTTCGTCA. For each oligonucleotide pair, a no-template control reaction was included.

Microarray analysis. Published microarray data [26] were used to compare gene expression levels in E14.5 $CD45^-$ $PECAM1^+$ brain versus pooled lung and liver ECs using GEO2R software (NCBI).

Statistical Analysis. Tissues for analysis were allocated to experimental groups according to genotype and gestational age. The number of YFP^+ ECs and YFP^+ microglia in *Csf1r-iCre;Rosa*^{Yfp} hindbrains (**Fig. 1a,b** and **1f-h**) was determined in three randomly chosen 0.72 mm^2 regions of each wholemount labelled and flatmounted hindbrain. For hindbrains in *Hoxa*-targeting experiments, the number of $F4/80^+$ microglia (**Extended Data Fig. 5**) and $tdTom^+$ and $IB4^+$ volume (**Fig. 5b,c**) were determined from confocal z-stacks of four randomly chosen 0.18 mm^2 regions on the lateral side of each hindbrain (**Extended Data Fig. 5g).** The z-stacks were surface rendered with Imaris (Bitplane) to obtain the $F4/80^+$, $tdTom^+$ and $IB4^+$ volumes, and the $F4/80^+$ volume was then subtracted from both the $IB4^+$ and $tdTom^+$ total volume to obtain the $IB4^+$ EC and $tdTom^+$ EC volume before calculating the ratio of $tdTom^+$ to $IB4^+$ EC volume. To determine the number of vascular intersections in *Hoxa*-targeting experiments (**Fig. 5b,d**), the same confocal z-stacks were analysed with Imaris filament tracer after $F4/80^+$ microglia were masked. For **Fig. 1** and **Fig. 5**, all counts obtained from one hindbrain were averaged to yield the value for that hindbrain; to ensure unbiased interpretation of results, the genotypes were disclosed only after data collection was complete. For all experiments, we calculated the mean value for at least 3 independent samples, where error bars represent the standard deviation of the mean (for details, see figure legends). Comparison of medians against means justified the use of a parametric test; to determine whether two datasets were significantly different, we therefore calculated p values with a two-tailed unpaired Student's t test; $P < 0.05$ was considered significant. When more than two data sets were compared, we used the statistical tests indicated in the associated figure legends. Statistical analyses were performed with Excel 12.2.6 (Microsoft Office) or Prism 5 (GraphPad Software).

References specific to the online methods

40. Srinivas, S. *et al.* Cre reporter strains produced by targeted insertion of EYFP and ECFP into the ROSA26 locus. *BMC Dev Biol* **1**, 4 (2001).
41. Madisen, L. *et al.* A robust and high-throughput Cre reporting and characterization system for the whole mouse brain. *Nature neuroscience* **13**, 133-140 (2010).
42. Kawamoto, S. *et al.* A novel reporter mouse strain that expresses enhanced green fluorescent protein upon Cre-mediated recombination. *FEBS letters* **470**, 263-268 (2000).
43. McKercher, S.R. *et al.* Targeted disruption of the PU.1 gene results in multiple hematopoietic abnormalities. *The EMBO journal* **15**, 5647-5658 (1996).
44. Zarkada, G., Heinolainen, K., Makinen, T., Kubota, Y. & Alitalo, K. VEGFR3 does not sustain retinal angiogenesis without VEGFR2. *Proceedings of the National Academy of Sciences of the United States of America* **112**, 761-766 (2015).
45. Yoshida, H. *et al.* The murine mutation osteopetrosis is in the coding region of the macrophage colony stimulating factor gene. *Nature* **345**, 442-444 (1990).
46. Vieira, J.M., Schwarz, Q. & Ruhrberg, C. Selective requirements for NRP1 ligands during neurovascular patterning. *Development* **134**, 1833-1843 (2007).
47. Goodell, M.A., Brose, K., Paradis, G., Conner, A.S. & Mulligan, R.C. Isolation and functional properties of murine hematopoietic stem cells that are replicating in vivo. *The Journal of experimental medicine* **183**, 1797-1806 (1996).
48. Bolger, A.M., Lohse, M. & Usadel, B. Trimmomatic: a flexible trimmer for Illumina sequence data. *Bioinformatics* **30**, 2114-2120 (2014).
49. Dobin, A. *et al.* STAR: ultrafast universal RNA-seq aligner. *Bioinformatics* **29**, 15-21 (2013).
50. Liao, Y., Smyth, G.K. & Shi, W. featureCounts: an efficient general purpose program for assigning sequence reads to genomic features. *Bioinformatics* **30**, 923-930 (2014).
51. Varet, H., Brillet-Gueguen, L., Coppee, J.Y. & Dillies, M.A. SARTools: A DESeq2- and EdgeR-Based R Pipeline for Comprehensive Differential Analysis of RNA-Seq Data. *PloS one* **11**, e0157022 (2016).

Extended data figure legends:

Extended data figure 1: Endothelial *Csf1r-iCre* targeting is observed with different recombination reporters and targeted ECs are distinguishable from macrophages and pericytes.

(**a-c**) Confocal z-stacks of *Csf1r-iCre;Rosa*^{Yfp} (**a**) *Csf1r-iCre;CAG-Cat-Egfp* (**b**) and *Csf1r-iCre;Rosa*^{tdTom} (**c**) hindbrains at the indicated stages were wholemount labelled with IB4 and YFP (**a**) or EGFP staining (**b**) or are shown together with tdTom fluorescence (**c**). In (**a**), the white squares indicate areas shown in higher magnification in **Fig. 1a**. The indicated single channels are also shown individually.

(**d,e**) Confocal z-stacks of E12.5 *Csf1r-iCre;Rosa*^{Yfp} hindbrains, wholemount labelled for YFP and the microglia marker F4/80 (**d**) or the pericyte marker NG2 (**e**) together with IB4 show that *Csf1r-iCre-targeted* vessel-bound cells are neither microglia nor pericytes. In (**d**), the boxed area is shown in higher magnification and as single channels adjacent to the panel. In (**e**), a single optical y/z cross section at the position indicated with the yellow line is displayed at higher magnification with single channels.

(**f**) Confocal z-stacks of a *Csf1r-iCre;Rosa*^{tdTom} E12.5 hindbrains, wholemount labelled for ERG and CDH5 and shown including tdTom fluorescence to demonstrate that *Csf1r-iCre* targets *bona fide* ECs that form junctions with neighbouring ECs.

Symbols: Microglia and ECs are indicated with arrowheads and arrows, respectively, pericytes with double arrowheads, junctional CDH5 staining with a curved arrow. Solid and clear symbols indicate the presence or absence of marker expression, respectively. *Scale bars*: 100 µm (**a**), 20 µm (**b-e**), 50 µm (**f**).

Extended data figure 2: Endothelial *Csf1r-iCre*-targeting is not caused by endothelial *Csf1r* expression and occurs independently of myeloid differentiation.

(**a,b**) Confocal z-stacks of E11.5 *Csf1r-iCre;Rosa*^{Yfp} (**a**) or *Csf1r-Egfp* (**b**) hindbrains, wholemount labelled for CSF1R and YFP or EGFP together with IB4, show lack of CSF1R protein and promoter activity in embryonic ECs.

(**c**) Graphic representation of relative *Cdh5* and *Csf1r* expression levels in E14.5 brain or pooled lung/liver EC microarrays [31]; n = 5 each; *** P > 0.001 (unpaired t-test).

(**d-f**) FACS separation of tdTom^{+} cells from *Csf1r-iCre;Rosa*^{tdTom} embryos, including (**d**) representative gating strategy to exclude dead cells and doublets in this and subsequent experiments and (**e**) sorting into PECAM1^{+} CD45^{-} ECs versus CD45^{+} PECAM1^{-} MCs for RT-qPCR analysis. (**f**) Representative gene amplification graphs for *Csf1r* versus *Actb* from tdTom^{+} MCs and

ECs; ΔRn, normalised reporter value for SYBR Green minus baseline instrument signals. (**g**) Graphic representation of the fold change in amplification of the indicated genes relative to *Actb* for both cell populations. Each data point represents the value of one embryo; n=3 each; * P > 0.05, *** P > 0.001 (unpaired t-test).

(**h**) Confocal z-stacks of *Csf1r-iCre;Rosa*^{Yfp} P0 striatum on a *Pu.1*$^{+/+}$ versus *Pu.1*$^{-/-}$ background, wholemount labelled for YFP and F4/80 together with IB4, show that *Csf1r-iCre*-targeted ECs are PU.1-independent.

Symbols: Arrowheads indicate microglia, arrows YFP^{+} ECs, clear arrows YFP^{+} ECs that are CSF1R^{-} and F4/80^{-}.

Scale bars: 20 μm.

Extended data figure 3: Lineage tracing of yolk sac and liver EMPs.

(**a,b**) Confocal z-stacks of wholemount labelled E8.5 wild type (**a**) and *Pu.1*$^{-/-}$ (**b**) yolk sacs on a *Csf1r-iCre;Rosa*^{Yfp} background, labelled for YFP and KIT, show *Csf1r-iCre*-targeted KIT^{+} round cells corresponding to EMPs/MPs and *Csf1r-iCre*-targeted KIT^{-} flat cells corresponding to ECs.

(**c-f**) Pregnant *Csf1r-Mer-iCre-Mer;Rosa*^{tdTom} (**c,d**) and *Kit*$^{CreERT2;}$*Rosa*^{tdTom} (**e,f**) dams were injected with a single tamoxifen dose on the indicated days; confocal z-stacks of E12.5 yolk sacs, immunolabelled for the indicated markers, show *Csf1r-iCre*-targeted ECs and macrophages.

Symbols: Wavy arrows indicate EMPs, straight arrows *Csf1r-iCre*-lineage traced ECs, arrowheads macrophages. Solid and clear symbols indicate the presence or absence, respectively, of the indicated markers. *Scale bars*: 20 μm.

(**g-i**) Pregnant dams were injected with a single tamoxifen dose on E10.5 (**g**) before analysis of E11.5 liver cells from *Csf1r-Egfp*;*Csf1r-Mer-iCre-Mer;Rosa*^{tdTom} (**h**; n=4 embryos) or *Csf1r-Mer-iCre-Mer;Rosa*^{tdTom} embryos lacking *Csf1r-Egfp* (**i**; n=4 embryos) by flow cytometry for CD45 and KIT; the CD45^{hi} KIT^{-} differentiated MC (blue), CD45^{lo} KIT^{+} EMP/myeloid progenitor (MP) (pink) and CD45^{-} KIT^{+} populations (grey) were gated further for *Csf1r-Egfp* and tdTom.

Extended data figure 4: Immunostaining controls for the analysis of cultured *Csf1r-iCre*-targeted cells.

The indicated cell populations were isolated by FACS from E12.5 *Csf1r-iCre;Rosa*^{tdTom} livers or blood and cultured for three days in methocult before adherent cells were stained. In the first panel in each row, the phase contrast and DAPI images were merged. In panels 2-4 in each row, immunolabelled cells are visualised together with tdTom fluorescence, with single channels for the indicated markers shown separately in grey scale. In (**a,b**), adherent cells from tdTom^{+} liver MC (**a**)

and EMP/MP (**b**) cultures were stained for ERG and VEGFR2 (top panels) or with secondary antibodies only (bottom panels). In (**c**), adherent cells from tdTom$^+$ blood EMP/MP cultures were immunostained for CSF1R together with the myeloid markers CD45 (top panels) or F4/80 (bottom panels). *Symbols*: Arrows indicate tdTom$^+$ ECs, arrowheads tdTom$^+$ myeloid cells. Solid and clear symbols indicate the presence or absence, respectively, of the indicated markers. *Abbreviations*: met, methocult; FN, fibronectin. *Scale bars*: 20 µm.

Extended data figure 5: *Csf1r-iCre*-mediated *Hoxa* ablation impairs the EMP lineage.

(**a-f**) Schematic representation of the *Hoxa* cluster and adjacent *Evx1* gene, including position of the *LoxP* sites used for gene targeting. (**b**) FACS strategy to isolate KIT$^+$ cells from control (pooled *Csf1r-iCre$^-$ or Csf1r-iCre$^+$;Hoxa$^{+/+}$*; n=14), *Hoxa$^{+/fl}$;Csf1r-iCre* heterozygous (n=6) and E12.5 *Hoxa$^{fl/fl}$;Csf1r-iCre* mutant livers (n = 8). (**c**) qPCR analysis of *Hoxa* gene copy number relative to *Evx1.* Data are shown as mean ± SD; each symbol represents the value for one individual liver; * P < 0.05, *** P < 0.001 (1-way ANOVA, Tukey's multiple comparisons test). (**d-f**) Representative FACS analysis (**d**) and quantification (**e,f**) of liver cell populations at E12.5 shows a similar number of CD45$^+$ or CD45$^+$ CD11b$^+$ cells (differentiated MCs) in control (pooled *Csf1r-iCre$^-$ or Csf1r-iCre$^+$;Hoxa$^{+/+}$*, n=25 for CD45$^+$ and n=17 for CD45$^+$ CD11b$^+$) versus *Hoxa$^{fl/fl}$;Csf1r-iCre* (n=7 for CD45$^+$ and n=6 for CD45$^+$ CD11b$^+$). Mean ± SD fold change in mutants compared to control; each data point represents the value for one hindbrain; ** P < 0.01; ns, non-significant (unpaired t-test).

(**g-i**) E12.5 hindbrains of the indicated genotypes were immunolabelled to determine vascular complexity and microglia. (**g**) Schematic representation of embryonic hindbrain position (left) and location of the hindbrain areas i-iv used for quantification in each hindbrain (right); values for the four areas in each hindbrain were averaged to obtain the value for that hindbrain; EC quantifications are shown in **Fig. 5c**. (**h**) Confocal z-stacks after wholemount labelling with IB4 and for RFP to visualise tdTom and F4/80 to visualise microglia; the white boxes indicate areas shown in higher magnification in **Fig. 5**. (**i**) Quantification of microglia number in *Hoxa$^{fl/fl}$;Csf1r-iCre* mutants (n=9) versus controls (n=10, pooled *Csf1r-iCre$^+$;Hoxa$^{+/+}$* and *Csf1r-iCre$^-$* of any *Hoxa* genotype). Mean ± SD fold change in mutant compared to control hindbrain; each data point represents the value for one hindbrain; ** P < 0.01 (unpaired t-test).

(**j-l**) Confocal z-stacks of E11.5 *Csf1$^{+/+}$* and *Csf1$^{+/op}$* littermate hindbrains, wholemount labelled for F4/80 together with IB4 (**j**) before quantification of the number of microglia (**k**) and vascular branchpoints (**l**); note that a 50% microglia reduction in *Csf1$^{+/op}$* compared to *Csf1$^{+/+}$* hindbrains did not reduce vascular complexity. Mean ± SD; each data point represents the value for one hindbrain, n=3 each; ** P < 0.01; ns, non-significant (unpaired t-test).

Scale bars: 200 µm (**h**), 100 µm (**j**).

Extended data figure 6: *Csf1r-iCre*-targeted ECs proliferate in vivo.

(**a,b**) Confocal z-stacks of E12.5 *Csf1r-iCre;Rosa*^{tdTom} wholemount yolk sac (**a**) or hindbrain (**b**) after staining for the proliferation marker pHH3 and VEGFR2 or for pHH3 together with IB4, respectively, and shown together with tdTom fluorescence. The areas indicated with white squares are shown in higher magnification below the corresponding panel, with tdTom and pHH3 channels also shown separately in grey scale. *Symbols*: The arrows indicate proliferating tdTom$^+$ pHH3$^+$ ECs. Solid and clear symbols indicate the presence or absence, respectively, of tdTom fluorescence. The wavy arrow indicates a tdTom$^-$ pHH3$^+$ neural progenitor. *Scale bars*: 200 µm (top panels), 20 µm (lower panels).

(**c-e**) *Cell cycle distribution of tdTom$^+$ and tdTom$^-$ ECs.* (**c**) FACS gating strategy to isolate tdTom$^+$ and tdTom$^-$ PECAM1$^+$ cells from *E12.5 Csf1r-iCre;Rosa*^{tdTom} embryos. (**d**) Graphic representation of cell distribution based on Hoechst 33342 fluorescence as a measure of DNA content; low and high staining intensity is observed in cells with a DNA ploidy of 2n, i.e. G0/G1 phase, or 4n, i.e. G2/M phase, respectively; an intermediate staining intensity corresponds to S phase. (**e**) Quantification of the proportion of tdTom$^+$ and tdTom$^-$ PECAM1$^+$ cells in the G1, S and G2/M phases based on the area of the corresponding peaks in (**d**). Mean ± SD, n = 3 each; n.s., non-significant (paired t-test).

Extended data figure 7: Validation of gene expression data from RNAseq and microarray studies.

ECs were isolated by FACS as in **Fig. 6a** for validation of RNAseq and microarray data presented in **Fig. 6d-f.**

(**a**) Relative transcript levels of the *Rosa26* locus by RNAseq of E12.5 tdTom$^+$ and tdTom$^-$ EC populations, whose analysis is presented in **Fig. 6a-f**; mean ± SD of normalised counts, n=3 each; ** P < 0.01 (unpaired t-test).

(**b**) RT-qPCR analysis for the indicated genes in tdTom$^+$ versus tdTom$^-$ ECs isolated from the whole embryo (n=5) to validate differentially expressed genes identified via RNAseq in **Fig. 6e,f**.

(**c**) RT-qPCR analysis for the indicated genes in tdTom$^-$ ECs isolated from the brain and liver (n=3 each) to validate organ-specific transcript enrichment identified via microarray analysis in **Fig. 6f**.

(**d**) RT-qPCR analysis for the indicated genes to directly compare the expression levels of brain and liver EC differentiation markers in tdTom$^+$ versus tdTom$^-$ ECs isolated from brain (n=3) or liver (n=5) (**d**) at E12.5.

Slc2a1 was analysed as a representative brain EC-enriched transcript/differentiation marker, *Mrc1* and *Oit3* as representative liver EC-enriched transcripts. Mean ± SD of fold change; * P < 0.05, ** P < 0.01, *** P < 0.001; ns, non-significant (unpaired t-test); ND, not detectable.

Extended data figure 8: *Csf1r-iCre*-targeted ECs contribute to embryonic organ vasculature.

(**a**) Cryosections of the indicated organs from E12.5 *Csf1r-iCre;Rosa*^{tdTom} mice were immunolabelled for the indicated EC markers together with antibodies for RFP to identify tdTom protein (top and bottom panels) or are shown with tdTom fluorescence (middle panels); single channels are shown in grey scale. The white boxes indicate the position of areas shown in higher magnification in **Fig. 6g**; note that some areas selected for higher magnification are not contained entirely within the field of view, and accordingly the boxes are not complete. *Scale bars:* 200 µm.

(**b**) Gating strategy for flow cytometry of dissociated cells from E12.5 *Csf1r-iCre;Rosa*^{tdTom} embryos and a control sample lacking *iCre* after staining with antibodies for CD11b, CD41, CD45, KIT, PECAM1 to determine the relative contribution of tdTom$^+$ versus tdTom$^-$ ECs to vasculature in the brain, lung, heart and liver (associated quantifications shown in **Fig. 6i**; an analogous strategy was used for the quantifications shown in **Fig. 6j** and in the **Extended Data Fig. 9b**).

Extended data figure 9: *Csf1r-iCre*-targeted ECs contribute to organ vasculature in late stage embryos.

(**a**) Cryosections of the indicated organs from E18.5 *Csf1r-iCre;Rosa*^{Yfp} mice were immunolabelled for YFP, PECAM1 and the macrophage marker IBA1; single channels are shown in grey scale. *Symbols*: Arrowheads indicate YFP$^+$ and IBA1$^+$ macrophages; solid and empty arrows indicate ECs that are YFP$^+$ and lack IBA1 expression, respectively. *Scale bars*: 20 µm.

(**b**) Flow cytometry of dissociated cells from the indicated organs of E18.5 *Csf1r-iCre;Rosa*^{tdTom} embryos after staining with antibodies for CD11b, CD41, CD45, KIT, PECAM1, using the gating strategy shown in the **Extended data Fig. 8a**; mean ± SD, n = 5 each; *** P > 0.001 (1-way ANOVA, Tukey's multiple comparisons test).

(**c**) Working model for the role of EMPs in generating extra-embryonic yolk sac and intra-embryonic organ ECs alongside their known role in generating myeloid and erythrocyte/megakaryocyte cells.

Extended data figure 10: *Csf1r-iCre*-targeted ECs contribute to adult organ vasculature.

Cryosections of the indicated organs from 6 months old adult *Csf1r-iCre;Rosa*^{Yfp} (**a**) or 3 months old adult *Csf1r-iCre;Rosa*^{tdTom} (**b**) mice were immunolabelled for the indicated EC and macrophage markers together with antibodies for YFP or RFP; single channels are shown in grey scale. The white box in (**b**) indicates an area shown in higher magnification in **Fig. 6h**. *Symbols*: Arrowheads indicate YFP$^+$ and F4/80$^+$ macrophages; solid and empty arrows indicate ECs that are YFP$^+$ and lack F4/80 expression, respectively. *Scale bars*: 20 µm (**a**), 100 µm (**b**).

a

Csf1r-iCre;Rosa^{Yfp}

Rosa^{Yfp} (no *iCre*)

E10.5 E11.5 E12.5 E12.5

YFP IB4

YFP

b

microglia

ECs

YFP$^+$ cells/0.72 mm^2

120 100 80 60 40 20 0

E10.5 E11.5 E12.5

c

vessel area (pixels x 10^5)

4 3 2 1

E12.5

E11.5

E10.5

r^2=0.91

0 20 40 60 80

YFP$^+$ ECs/0.72 mm^2

d

Csf1r-Mer-iCre-Mer; Rosa^{tdTom}

E12.5

tdTom IB4

tam @ E10.5

tdTom

e

Csf1r-iCre;Rosa^{tdTom} Cdh5-Cre^{ER};Rosa^{tdTom}

E12.5

tam @ E11.5

tdTom tdTom

ERG ERG

PECAM1 PECAM1

tdTom ERG PECAM1

f

E11.5 *Csf1r-iCre;Rosa^{Yfp}*

YFP F4/80

YFP F4/80

Pu.1$^{+/+}$

Pu.1$^{-/-}$

YFP IB4

g

3D surface rendering

lu

h

YFP$^+$ microglia/0.72mm^2

100 80 60 40 20 0

***

Pu.1$^{+/+}$ *Pu.1$^{-/-}$*

YFP$^+$ ECs/0.72mm^2

50 40 30 20 10 0

n.s.

Pu.1$^{+/+}$ *Pu.1$^{-/-}$*

a

E8.5 *Csf1r-Egfp*

EGFP VEGFR2

EGFP

3D rendering

lu

lu

b

E8.5 *Csf1r-iCre;Rosa*^{Yfp}

YFP VEGFR2

YFP

3D rendering

lu

lu

lu

E8.5 *Pu.1*$^{-/-}$*;Csf1r-iCre;Rosa*^{Yfp}

YFP VEGFR2

YFP

3D rendering

lu

lu

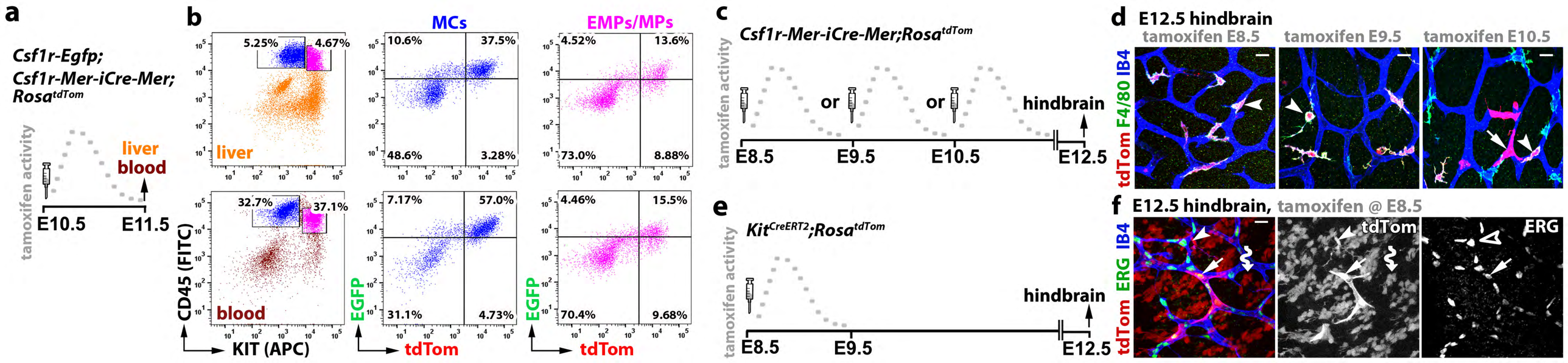
a
Csf1r-Egfp;
Csf1r-Mer-iCre-Mer;
Rosa^tdTom
tamoxifen activity
liver
blood
E10.5
E11.5
b
MCs
EMPs/MPs
5.25%
4.67%
liver
10.6%
37.5%
48.6%
3.28%
4.52%
13.6%
73.0%
8.88%
32.7%
37.1%
blood
7.17%
57.0%
31.1%
4.73%
4.46%
15.5%
70.4%
9.68%
CD45 (FITC)
KIT (APC)
EGFP
tdTom
EGFP
tdTom
c
Csf1r-Mer-iCre-Mer;Rosa^tdTom
tamoxifen activity
or
or
hindbrain
E8.5
E9.5
E10.5
E12.5
d
E12.5 hindbrain
tamoxifen E8.5
tamoxifen E9.5
tamoxifen E10.5
tdTom F4/80 IB4
e
Kit^CreERT2;Rosa^tdTom
tamoxifen activity
hindbrain
E8.5
E9.5
E12.5
f
E12.5 hindbrain, tamoxifen @ E8.5
tdTom ERG IB4
tdTom
ERG

a

Csf1r-iCre;Rosa^{tdTom}
E12.5

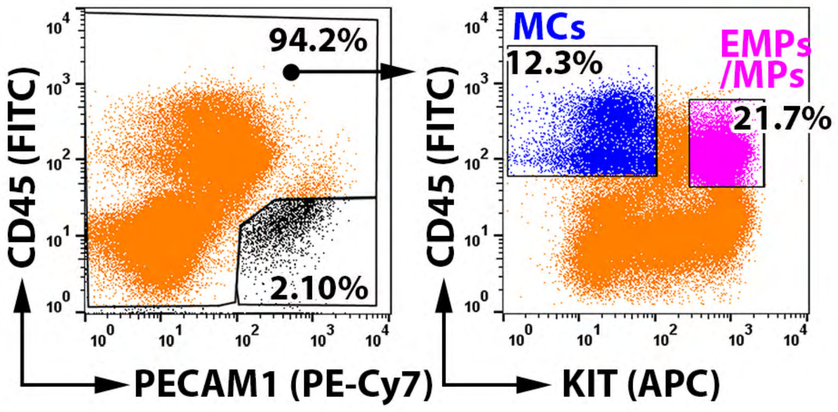

b

Csf1r-iCre;Rosa^{tdTom}
E12.5

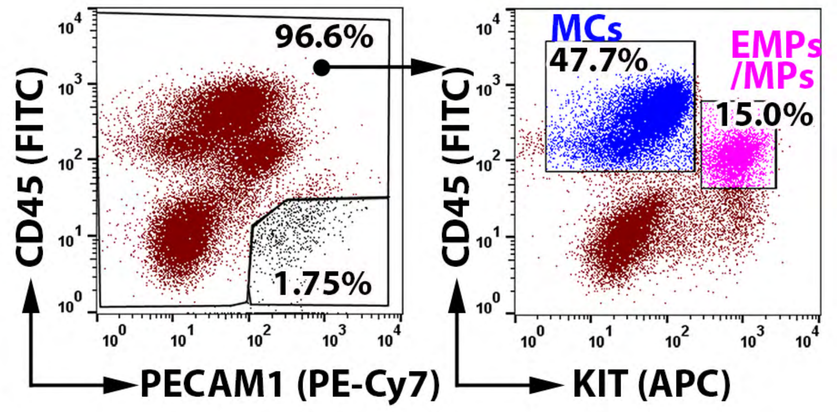

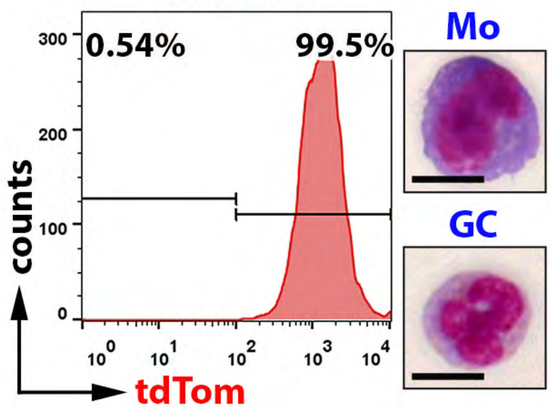

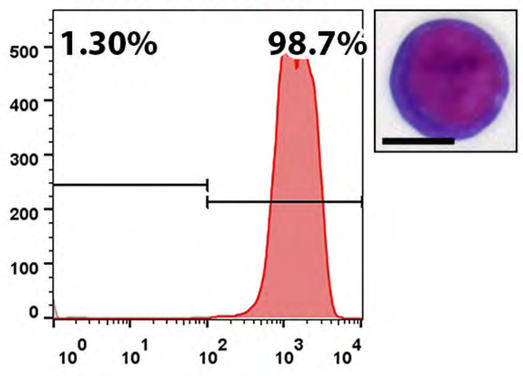

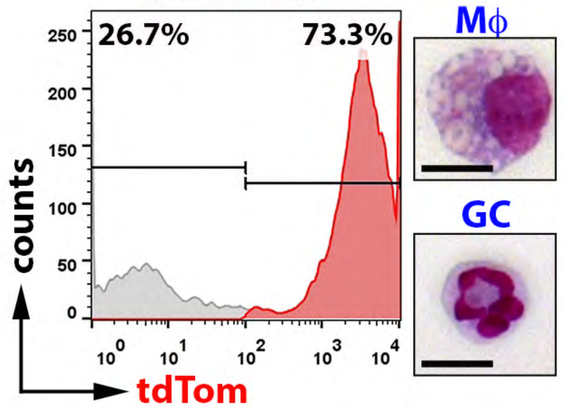

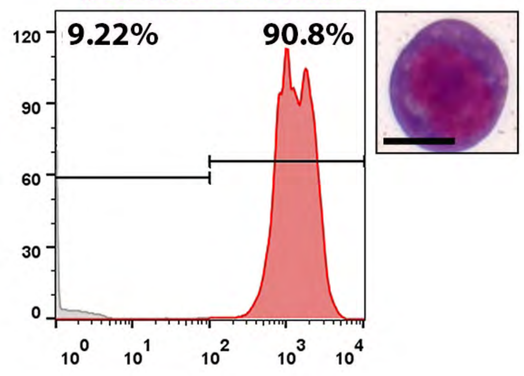

c

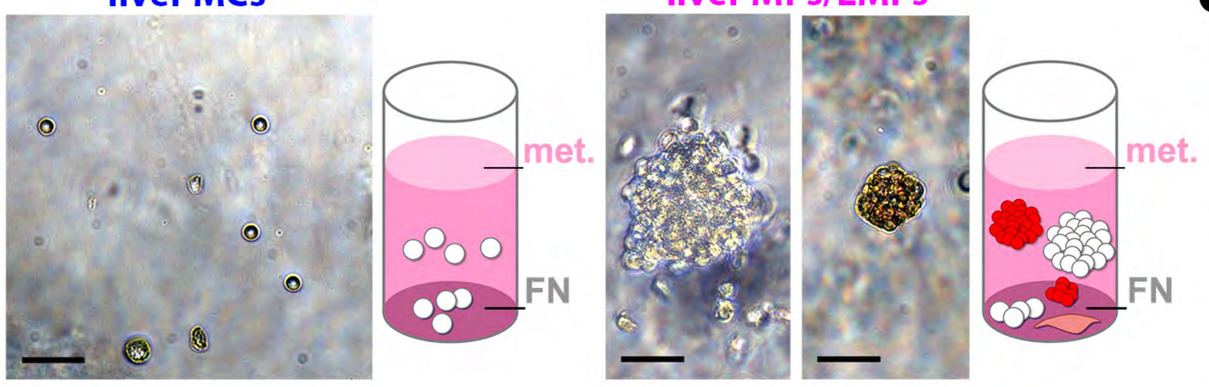

d

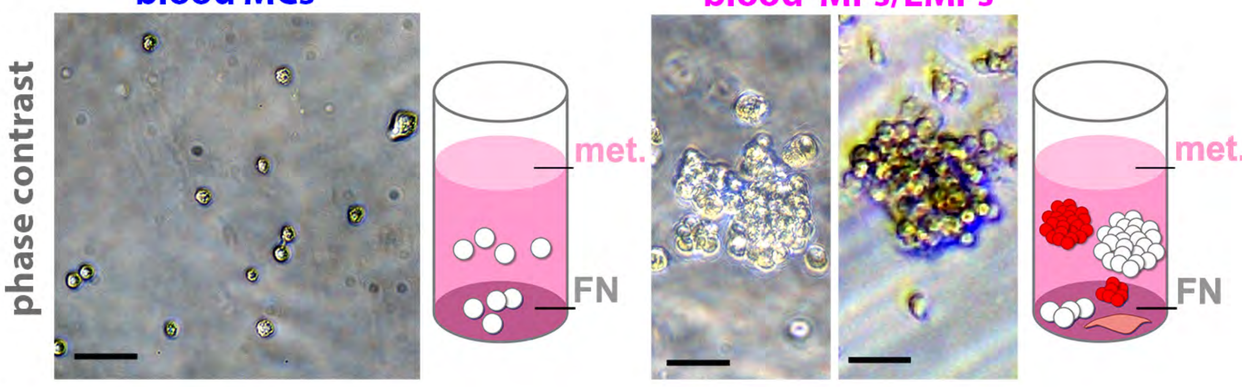

e

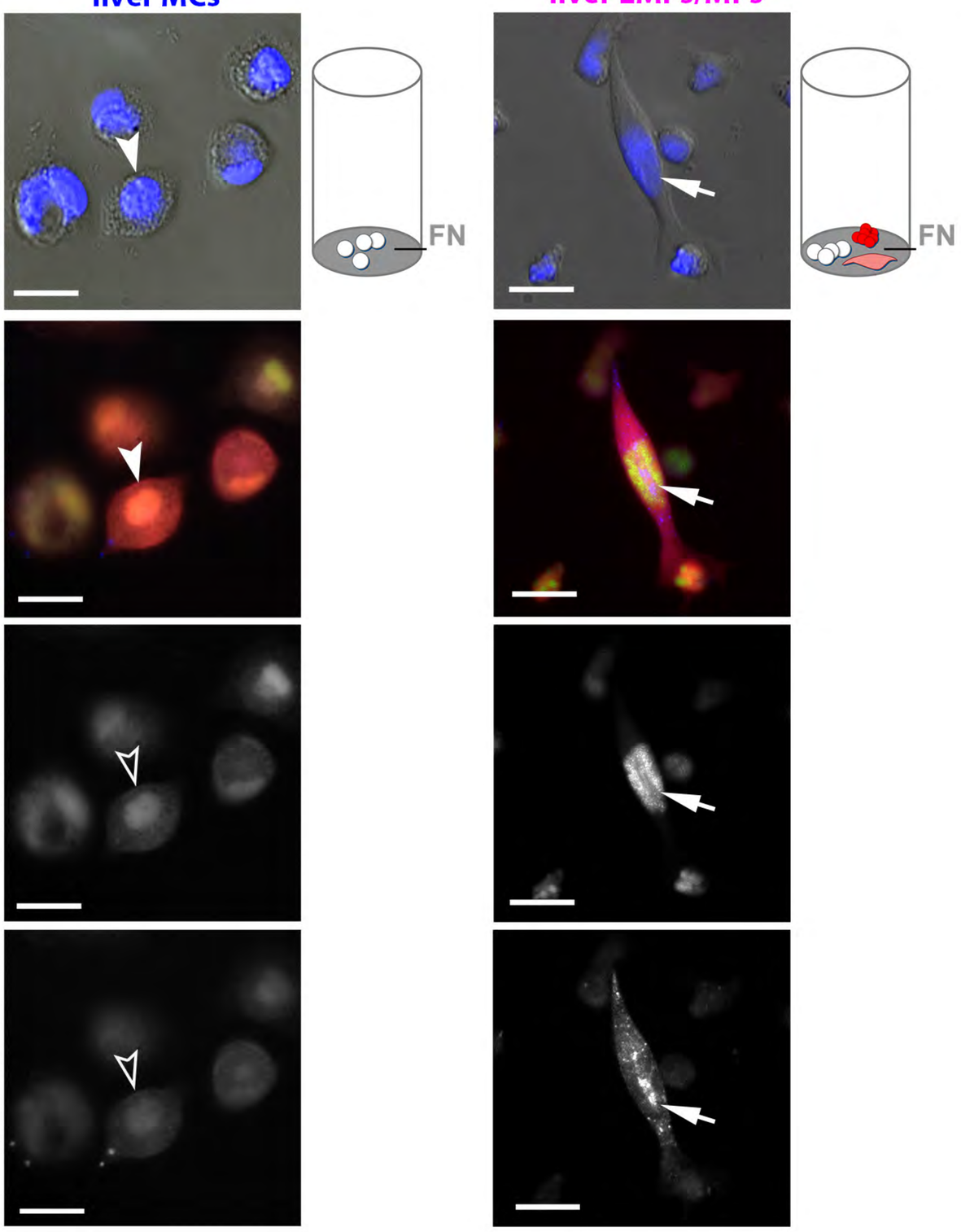

f

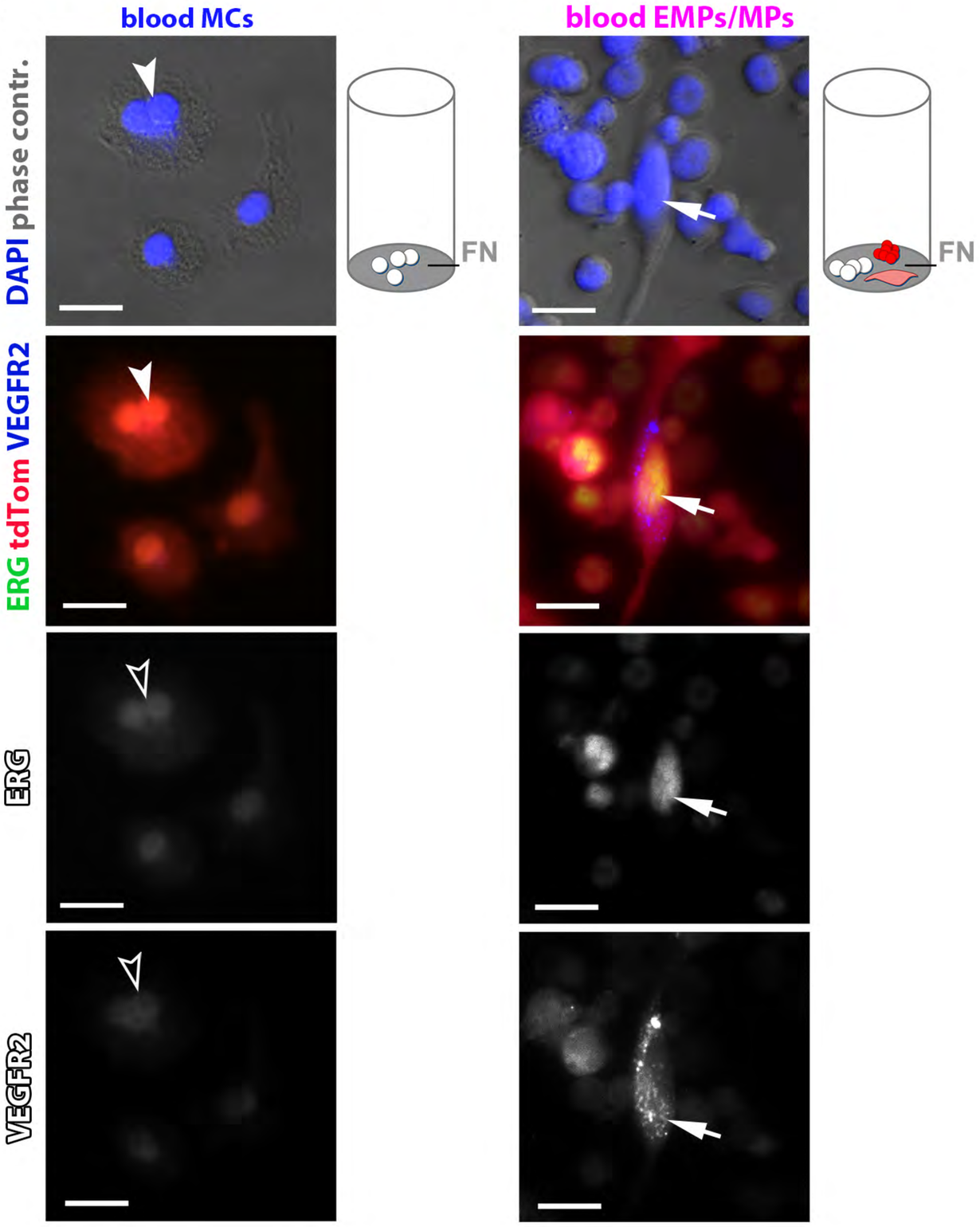

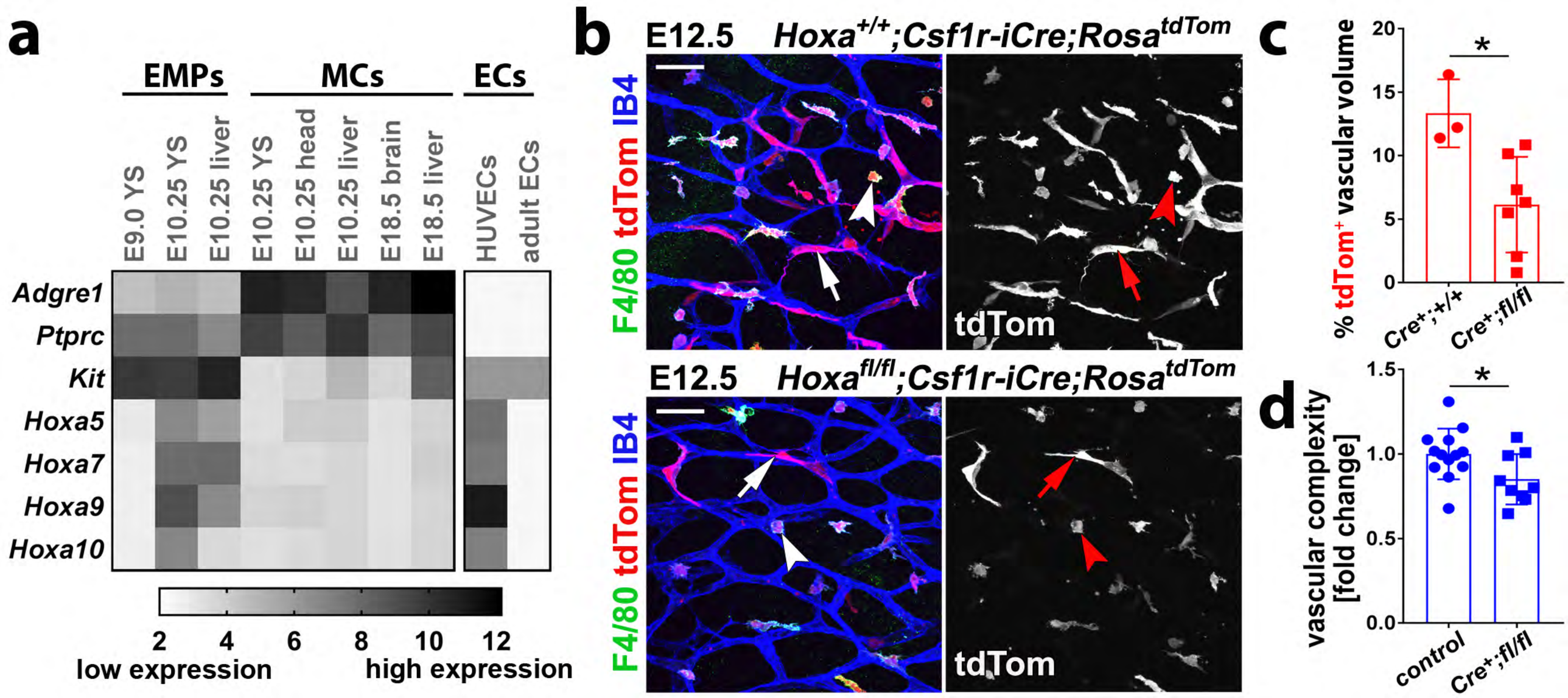
a
EMPs
MCs
ECs
E9.0 YS
E10.25 YS
E10.25 liver
E10.25 YS
E10.25 head
E10.25 liver
E18.5 brain
E18.5 liver
HUVECs
adult ECs
Adgre1
Ptprc
Kit
Hoxa5
Hoxa7
Hoxa9
Hoxa10
2
4
6
8
10
12
low expression
high expression
b
E12.5 Hoxa+/+;Csf1r-iCre;RosatdTom
F4/80 tdTom IB4
tdTom
E12.5 Hoxafl/fl;Csf1r-iCre;RosatdTom
F4/80 tdTom IB4
tdTom
c
% tdTom+ vascular volume
20
15
10
5
0
*
Cre+;+/+
Cre+;fl/fl
d
vascular complexity [fold change]
1.5
1.0
0.5
0.0
*
control
Cre+;fl/fl

a
E12.5 *Csf1r-iCre;Rosa*^{tdTom} (whole embryo)
CD45 (FITC)
CD11b (PERCP-Cy5.5)
91.1%
CD45$^-$ CD11b$^-$
KIT (APC)
PECAM1 (PE-Cy7)
3.41%
KIT$^-$ PECAM1$^+$
count
tdTom
72.6%
27.4%
b
adjP<0.05
adjP>0.05
tdTom$^-$ ECs (counts)
tdTom$^+$ ECs (counts)
c
up in tdTom$^+$ ECs
up in tdTom$^-$ ECs
adjP<0.05
exp>100
n=247
tdTom$^-$ ECs (counts)
Log$_2$FC
Oit3
Gpr182
Stab2
Cxcl10
Mrc1
Itga2b
Eln
Fbln2
Wnt4
Adamts8
Dppa5a
n=37
n=77
d
non-EC transcripts
tdTom$^-$ ECs
tdTom$^+$ ECs
Cx3cr1
Csf1r
Adgre1
Aif1
Itgam
Ptprc
Gfap
Acta2
Rbfox3
Nefl
Myog
Cdh1
ns
counts
e
core EC transcripts
tdTom$^-$ ECs
tdTom$^+$ ECs
Erg
Tjp2
Dll4
Tjp1
Icam1
Icam2
Cldn5
Flt1
Nrp1
Cdh5
Emcn
Tek
Pecam1
Kdr
Plvap
counts
EC maturation transcripts
Efnb2
Ephb3
Epha7
Wnt11
Wnt4
Fbln5
Fbln2
Eln
Col9a1
counts
f
brain EC transcripts
tdTom$^-$ ECs
tdTom$^+$ ECs
Fzd2
Col9a2
Adamts8
Dppa5a
Zic3
Slc7a5
Mfsd2a
Lef1
Abcb1a
Slc2a1
counts
E14.5 brain ECs
E14.5 liver/lung ECs
Log$_2$OD
liver EC transcripts
Gata1
Gp1ba
Plek
Itgb3
Itga2b
Nfe2
Gp5
Pf4
Ly6a
Cxcl10
Irf8
Mrc1
Lyve1
Gata4
Oit3
Stab2
Gpr182
counts
Log$_2$OD
g
E12.5 liver, *Csf1r-iCre;Rosa*^{tdTom}
F4/80 tdTom VEGFR2
VEGFR2
LYVE1 tdTom VEGFR2
LYVE1
MRC1 tdTom ERG
MRC1
h
adult liver, *Csf1r-iCre;Rosa*^{tdTom}
F4/80 tdTom VEGFR2
VEGFR2
LYVE1 tdTom VEGFR2
LYVE1
MRC1 tdTom DAPI
MRC1
i
% tdTom$^+$ ECs (E12.5)
brain
heart
lung
liver
j
% tdTom$^+$ ECs (adult)
brain
heart
lung
liver